Developmental Biology 452 (2019) 21–33

Contents lists available at ScienceDirect

Developmental Biology

journal homepage: www.elsevier.com/locate/developmentalbiology

Original research article

Microtubules are required for the maintenance of planar cell polarity in monociliated floorplate cells

Andrew W. Mathewson [a,b], Daniel G. Berman [a,c], Cecilia B. Moens [a,b,c,*]

[a] Division of Basic Sciences, Fred Hutchinson Cancer Research Center, Seattle, WA, USA
[b] Molecular and Cellular Biology Graduate Program, University of Washington, Seattle, WA, USA
[c] Biology Graduate Program, University of Washington, Seattle, WA, USA

A B S T R A C T

The asymmetric localization of planar cell polarity (PCP) proteins is essential for the establishment of many planar polarized cellular processes, but the mechanisms that maintain these asymmetric distributions remain poorly understood. A body of evidence has tied oriented subapical microtubules (MTs) to the establishment of PCP protein polarity, yet recent studies have suggested that the MT cytoskeleton is later dispensable for the maintenance of this asymmetry. As MTs underlie the vesicular trafficking of membrane-bound proteins within cells, the requirement for MTs in the maintenance of PCP merited further investigation. We investigated the complex interactions between PCP proteins and the MT cytoskeleton in the polarized context of the floorplate of the zebrafish neural tube. We demonstrated that the progressive posterior polarization of the primary cilia of floorplate cells requires not only Vangl2 but also Fzd3a. We determined that GFP-Vangl2 asymmetrically localizes to anterior membranes whereas Fzd3a-GFP does not polarize on anterior or posterior membranes but maintains a cytosolic enrichment at the base of the primary cilium. Vesicular Fzd3a-GFP is rapidly trafficked along MTs primarily toward the apical membrane during a period of PCP maintenance, whereas vesicular GFP-Vangl2 is less frequently observed. Nocodazole-induced loss of MT polymerization disrupts basal body positioning as well as GFP-Vangl2 localization and reduces cytosolic Fzd3a-GFP movements. Removal of nocodazole after MT disruption restores MT polymerization but does not restore basal body polarity. Interestingly, GFP-Vangl2 repolarizes to anterior membranes and vesicular Fzd3a-GFP dynamics recover after multiple hours of recovery, even in the context of unpolarized basal bodies. Together our findings challenge previous work by revealing an ongoing role for MT-dependent transport of PCP proteins in maintaining both cellular and PCP protein asymmetry during development.

1. Introduction

Cellular polarization is a fundamental aspect of animal development that enables epithelial cells to organize intracellularly to perform specialized functions appropriate for their tissue context. Epithelia exhibit two types of cellular polarity: apicobasal polarity, which defines the axis between the apical and basal membranes, and planar polarity, which is polarization in the plane of the epithelium, orthogonal to the apicobasal axis. *Drosophila* mutants that displayed misoriented and supernumerary actin-based hairs on the adult wing identified a core set of proteins that define the Planar Cell Polarity signaling pathway (Gubb and Garcia-Bellido, 1982). A highly conserved signaling pathway, PCP has been implicated in a number of developmental processes including the orientation of mammalian skin hair follicles (Devenport and Fuchs, 2008) and inner ear sensory hair cells (Etheridge et al., 2008; Montcouquiol et al., 2003); the directed migration of neurons and axons (Davey and Moens, 2017) and the collective movements of cells during gastrulation (Heisenberg et al., 2000; Tada and Smith, 2000; Wallingford and Harland, 2001) and neural tube closure (Curtin et al., 2003; Wallingford and Harland, 2001; Wang et al., 2006; Butler and Wallingford, 2018) as well as cilia positioning and directional beating in trachea (Vladar et al., 2012) oviducts (Shi et al., 2014, 2016) and in the central nervous system (Borovina et al., 2010; Boutin et al., 2014).

The PCP signaling pathway functions at the protein level to polarize subcellular information intracellularly and propagate this information through direct cell-cell interactions, which result in locally coordinated tissue polarity (Tree et al., 2002). The core PCP pathway in fly wing disc cells is composed of two membrane-localized protein complexes: the Frizzled (Fz or Fzd in vertebrates) complex consisting of Fz, Dishevelled (Dsh or Dvl in vertebrates), and Diego (Dg, or Diversin in vertebrates); and the Van Gogh (Vang, or Vangl in vertebrates) complex consisting of Vang and Prickle (Pk) (for review see (Goodrich and Strutt, 2011)). Through intracellular destabilizing interactions and intercellular stabilizing interactions, these PCP protein complexes sort into complementary membrane domains at the cell cortex, with the Fz complex localizing to distal membranes and the Vang complex to proximal membranes (Strutt et al., 2002; Strutt and Strutt, 2007). Flamingo (Fmi or Celsr in vertebrates), localizes to both proximal and distal membranes and is essential for mediating the intercellular interactions between the Fz and Vang complexes (Shimada et al., 2001). This asymmetric localization of core

* Corresponding author. Division of Basic Sciences, Fred Hutchinson Cancer Research Center, Seattle, WA, USA.
E-mail address: cmoens@fredhutch.org (C.B. Moens).

https://doi.org/10.1016/j.ydbio.2019.04.007
Received 8 November 2018; Received in revised form 6 April 2019; Accepted 9 April 2019
Available online 25 April 2019

PCP protein complexes, which can best be visualized using mosaically expressed, fluorescently tagged PCP proteins, also underlies the planar polarization of vertebrate epithelia including that of the neuroepithelium and floorplate (Butler and Wallingford, 2015; Davey et al., 2016; Deans et al., 2007; Devenport and Fuchs, 2008; Montcouquiol et al., 2006; Vladar et al., 2012; Butler and Wallingford, 2018).

Microtubules (MTs) have been implicated in the establishment of planar polarity. In the fly wing, a slight bias in plus-end MT orientation toward the distal side of cells biases the kinesin-based trafficking of vesicles containing Fmi, Fz, and Dsh distally, initiating an asymmetry which is then amplified by the intracellular destabilizing and extracellular stabilizing interactions between the core PCP complexes mentioned above (Harumoto et al., 2010; Olofsson et al., 2014; Shimada et al., 2006). This amplification process is also thought to involve MTs when membrane-bound complexes are endocytosed and trafficked either back to the membrane or to lysosomes for degradation in a process known as "endocytic flux" (Classen et al., 2005; Mottola et al., 2010; Strutt and Strutt, 2008) (for review see (Butler and Wallingford, 2017)). The polarized distribution of PCP core components is only transient in Drosophila epithelia, so the mechanisms that maintain stable planar polarity have not been investigated in this model.

Multiple recent studies have suggested that a role for MT networks in the establishment of PCP protein asymmetry is conserved in vertebrates, yet this work also suggests that MTs are subsequently dispensable for the maintenance of PCP protein asymmetry (Boutin et al., 2014; Chien et al., 2015; Sepich et al., 2011; Shi et al., 2016; Vladar et al., 2012). This is surprising, as endocytic flux of membrane-associated proteins is a ubiquitous and ongoing process within living cells, and trafficking of protein-containing vesicles along MTs is expected to be an integral part of this process (Butler and Wallingford, 2017). Maintenance of asymmetric PCP protein localization may be essential for ongoing planar polarized cellular processes including neuronal migration (Davey and Moens, 2017), but the mechanism by which any cell type maintains PCP asymmetry is unknown. Our ability to visualize the *in vivo* dynamics of PCP and MT fluorescent fusion proteins after cellular PCP has been established makes the zebrafish floorplate an ideal model for the study of the complex interactions between PCP proteins, the MT cytoskeleton, and maintenance of polarized cellular architecture.

In this work we describe the progressive establishment and subsequent maintenance of planar cell polarity in the zebrafish floorplate as detected by the posterior localization of the primary cilia and the asymmetric localization of PCP proteins Vangl2 and Fzd3a. Although we recognize that there are both cellular and molecular aspects to both ciliary polarity and PCP protein polarity, for simplicity hereafter we refer to the asymmetric localization of the primary cilium as "cellular polarity" and the asymmetric distribution of PCP proteins as "molecular polarity". We find that GFP-Vangl2 protein asymmetrically localizes to anterior membranes whereas Fzd3a-GFP is primarily detectable in dynamic vesicles that traffic along MTs toward the base of the primary cilium. Contrary to prior studies, we find that MTs are required to maintain both cellular and molecular polarity after it is established in the floorplate. Molecular but not cellular polarity is re-established after recovery of MTs, demonstrating that in this system the asymmetric position of the MTOC does not appear to feed back on the polarized localization of PCP proteins as has been proposed in other planar polarized epithelia. Our findings challenge previous work by revealing an ongoing role for MT-dependent transport of PCP proteins in maintaining both cellular and molecular asymmetry during development.

2. Methods

2.1. Ethics statement

The Fred Hutchinson Cancer Research Center Institutional Animal Care and Use Committee (IACUC) follow the guidelines of the Office of Laboratory Animal Welfare and set its policies according to The Guide for the Care and Use of Laboratory Animals. Fred Hutchinson Cancer Research Center maintains full accreditation from the Association for Assessment and Accreditation of Laboratory Animal Care (AAALAC) and has letters of assurance on file with OLAW. The IACUC routinely evaluates the Fred Hutchinson animal facilities and programs to assure compliance with federal, state, local, and institution laws, regulations, and policies. The OLAW Assurance number is D16-00142.

2.2. Zebrafish lines and maintenance

Zebrafish (*Danio rerio*) were raised at the Fred Hutchinson Cancer Research Center, and animal care and experiments were approved by the Institutional Animal Care and Use Committee. All animals were maintained according to standard procedures (Westerfield, 2000) and staged as previously described (Kimmel et al., 1995). All mutant lines used were previously described and are registered at The Zebrafish International Resource Center (ZIRC): *fzd3a*^{rw689} (*olt*^{rw689}) (Wada et al., 2006) and *vangl2*^{m209} (*tri*^{m209}) (Jessen et al., 2002).

2.3. Cloning and transgenic line generation

The following transgenic lines were generated for this study: *Tg(shha-gata2a:gal4-vp16)fh386* (Davey et al., 2016), *Tg(uas:GFP-Vangl2)fh453, Tg(uas:mkate2-Vangl2)fh496, Tg(uas:Fzd3a-GFP)fh447, Tg(uas:Fzd3a-mEOS)fh499, Tg(uas:EB3-mkate2)fh500, Tg(uas:p50p2a-eGFPCAAX) fh501*. Transgenic elements were cloned using the Gateway (Life Technologies) system using the gene specific primer sequences listed in Supp. Table 1. Final DNA constructs were assembled in the pDESTpBHR4R3 plasmid (gift from the Brockerhoff Lab). Transgenic embryos were generated by Tol2 transposase RNA co-injection with each plasmid at the single cell stage (Kawakami et al., 2000).

2.4. Drug treatments

Nocodazole treatments were done using a modified protocol from (McFarland et al., 2017). Briefly, nocodazole (Sigma) solutions were prepared fresh in DMSO and diluted in embryo media (Westerfield, 2000) with final concentrations of 5 ng/mL and placed on ice. Embryos were anesthetized and placed in 60 mm polystyrene petri dishes (Fisher Scientific) on ice. Embryo media was removed from embryos and replaced with 3 mL ice cold nocodazole or DMSO solution for the duration of drug treatment. Embryos were removed from ice after treatment and were either fixed immediately or washed at least 4x in room-temperature embryo media. Embryo recovery periods occurred in embryo media in a 28 °C incubator. Importantly, within minutes of removal from ice, treated embryos fully recover from multiple hours on ice based on motility and responsiveness to touch (data not shown).

2.5. Whole-mount immunohistochemistry

Anesthetized zebrafish embryos were fixed in 2% trichloroacetic (TCA) acid for 3 h or 4% paraformaldehyde (PFA)/4% sucrose in PBS for 1 h at room temperature. Fixed tissue was washed in PBS + 0.5% TritonX100, brain tissue was dissected and then blocked by standard antibody incubations. Following staining, tissue was cleared step-wise in a 25%, 50%, 75% glycerol series and mounted for confocal imaging. The following antibodies were used: chicken anti-GFP (1:500, Abcam Cat# ab13970); rabbit anti-ZO-1 (1:500, Zymed Cat# 61–7300); mouse anti-Cc2d2a (1:100, (Bachmann-Gagescu et al., 2011)); rabbit anti-RFP (1:1000, Abcam Cat# ab62341) (cross reacts with mkate2); mouse anti-acetylated tubulin (1:2000, Sigma Aldrich Cat# T6793) and rabbit anti-alpha tyrosinated tubulin (1:500, Millipore Cat# ABT171).

2.6. Imaging and data analysis

Imaging was performed using a Zeiss 700 confocal microscope with a

40x C-Apochromat 1,2 W-Korr UV–Vis-IR water immersion objective with the Zen 2010 software package. BB Polarity indices were determined by dividing the distance between the anterior cell membrane and the position of the BB by the distance between the anterior and posterior membranes at the level of the BB. For time-lapse imaging, short Z-stack images at 0.50 μm steps were captured every 5 s until photobleaching of fluorescent proteins hindered image acquisition. Live lateral imaging was limited to floorplate cells in the posterior halves of animals as the increased body thickness of the anterior halves of embryos obscures imaging of the medially located floorplate. Imaging of fluorescent fusion proteins was performed in isolated expressing cells in mosaically expressing embryos generated via plasmid injection or in stable transgenic lines that exhibited UAS silencing (Goll et al., 2009). Z-stacks of whole cell fluorescence were obtained and analyzed for polarized GFP-Vangl2 or Fzd3a-GFP localization. Anterior versus posterior asymmetry of GFP-Vangl2 and Fzd3a-GFP localization was measured by drawing ROIs on cell anterior and posterior halves and recording average pixel intensity with the plot profile tool in ImageJ (schematic, Fig. 2c). Anterior versus posterior membrane enrichment of GFP-Vangl2 and Fzd3a-GFP was determined by measuring fluorescence intensities of maximum intensity projections using a 1 μm wide trace along anterior and posterior membranes in ImageJ (schematic, Fig. 2d). To visualize Fzd3a localization in the context of p50-p2a-eGFPCAAX we photoconverted Fzd3a-mEOS to red fluorescence. As p2a sequences are cleaved during translation (Kim et al., 2011) we used eGFPCAAX localization to determine the position of the primary cilia along the apical membranes of floorplate cells co-expressing both transgenes. Fzd3a-GFP puncta dynamics were tracked and recorded using the MTrackJ plugin in ImageJ (Meijering et al., 2012). Movies were corrected for bleaching and levels were adjusted in ImageJ. All movies were exported as AVIs at 7 frames/sec. Graphs were generated and statistics were computed using GraphPad Prism software. All statistical analyses were performed using a 95% confidence interval. Figure images and diagrams were created using Zeiss Zen software, ImageJ, Adobe Photoshop CC, and Adobe Illustrator CC.

2.7. Kymographs

Kymographs of Fzd3a-GFP vesicular trafficking along MT tracks were generated in ImageJ from time-lapse movies by tracing 1 μm wide segmented user-drawn lines along MTs that were then superimposed on the corresponding fluorescently labeled PCP protein channel, straightened, and then timepoints were combined into montages. Kymograph traces were generated using the multi-kymograph overlay ImageJ plugin.

2.8. Rose-plots

Overall vesicle displacement directionality was determined by measuring the angle between the first and last positions of tracked Fzd3a-GFP vesicles. Rose plots were generated using the polarhistogram function in MatLab (https://www.mathworks.com/help/matlab/ref/polarhistogram.html). Outer plot numbers reflect relative angle of displacement while internal numbers indicate number of vesicles counted that were displaced at those relative angles, grouped into 15° bins. Apical movement defined as displacement between 45 and 135°, anterior defined as 135–225°, basal defined as 225–315°, and posterior defined as 315 to 45°.

3. Results

3.1. The floorplate is progressively planar polarized in a Vangl2 and Fzd3a-dependent manner

Previous studies establish that the apically docked BB of the primary cilium becomes asymmetrically localized toward the posterior side of floorplate cells in zebrafish by two days post-fertilization (dpf), and that this polarity requires planar cell polarity (PCP) signaling (Borovina et al., 2010; Davey et al., 2016; Walsh et al., 2011) (Fig. 1a–d). The position of the primary cilium can be visualized *in vivo* through live lateral imaging of floorplate cells expressing membrane-localized fluorescent proteins using the Tg(*shha-gata2a:gal4-vp16*) transgenic driver, henceforth referred to for simplicity as Tg(*shh:gal4*) (Fig. 1a,c, Supp Movie 1) (Davey et al., 2016; Ertzer et al., 2007) The position of the BB can be precisely determined in a ventral view of the fixed, dissected spinal cord using an antibody to Cd2d2a which localizes ~100 nm distal to the BB in the ciliary transition zone (Bachmann-Gagescu et al., 2011; Shi et al., 2017) (Fig. 1d). For the purposes of this work we assume henceforth that the BB lies at the base of the primary cilium and co-localizes with Cc2d2a. To understand the timing during which the BB becomes posteriorly localized, we assessed BB localization in fixed embryos at various stages of development. As early as the 10-somite stage (ss), the initial timepoint at which we can identify and image floorplate cells in the developing embryo, BBs within floorplate cells have docked apically and are localized posteriorly (Fig. 1e; polarity index: 0.72, $n = 125$ cells, 12 embryos; polarity index is the ratio of the distance from the anterior cell membrane to the BB over the total anterior-posterior length of the cell along the same line, averaged from ten floorplate cells per embryo; see methods). This early appearance of planar polarity is not unexpected given that the planar polarized distribution of PCP proteins is detectable in the neural plate and is required for neural tube closure (Butler and Wallingford, 2018). The BB becomes progressively more posteriorly localized from the 10ss until 30 h-post-fertilization (hpf), at which point BBs display a polarity index of 0.84 ($n = 206$ cells, 12 embryos). After this time the position of the BB is maintained through the end of our analysis at 72hpf ($p > 0.9999$, $n = 100$ cells, 10 embryos) (Fig. 1e). We thus define the period between 30 and 72 hpf as the maintenance phase of floorplate planar polarity.

Supplementary video related to this article can be found at https://doi.org/10.1016/j.ydbio.2019.04.007.

Floorplate planar polarization is critically dependent on the core PCP transmembrane protein Vangl2 as has been shown previously (Borovina et al., 2010; Davey et al., 2016), and we quantified this requirement using our polarity index measurement at 48 hpf (polarity index in *vangl2*^{m209} mutants is 0.47, $p < 0.0001$, $n = 100$ cells, 10 embryos) (Fig. 1g). We also found that the opposing transmembrane core component, Fzd3a, is required for floorplate planar polarization, although less dramatically, suggesting a possible redundancy with other Fzd proteins in the floorplate (polarity index *in fzd3a*^{rw689}: 0.67, $p = 0.0018$, $n = 198$ cells, 19 embryos) (Fig. 1f and g). Taken together, we find that the zebrafish floorplate becomes progressively polarized through a Fzd3a and Vangl2-dependent mechanism that positions BBs near the posterior apical membrane by 30hpf, and that this polarity is maintained at least until 72hpf.

3.2. Vangl2 and Fzd3a localization in the floorplate

One of the characteristics of the PCP pathway is that cellular asymmetry, which in the floorplate is reflected in the position of the BB, is underlain by molecular asymmetry of the PCP core components themselves. To understand how floorplate cellular asymmetry is established and maintained, we examined the dynamics of Vangl2 and Fzd3a localization in live zebrafish embryos using fluorescent fusion proteins. Use of mosaic expression of fusion proteins to visualize PCP protein distributions in vertebrate epithelia enables anterior and posterior membranes of irregularly shaped cells to be distinguished from the membranes of adjacent non-expressing cells (Butler and Wallingford, 2015; Ciruna et al., 2006; Davey et al., 2016; Devenport and Fuchs, 2008; Devenport et al., 2011; Roszko et al., 2009). Furthermore, PCP protein expression is widespread in the embryo, necessitating tissue-specific drivers to assess their sub-cellular localization, particularly in deep tissues like the floorplate. We previously reported that within the floorplate, GFP-Vangl2 (corroborated by Vangl2 immunostaining) and Fzd3a-GFP are planar

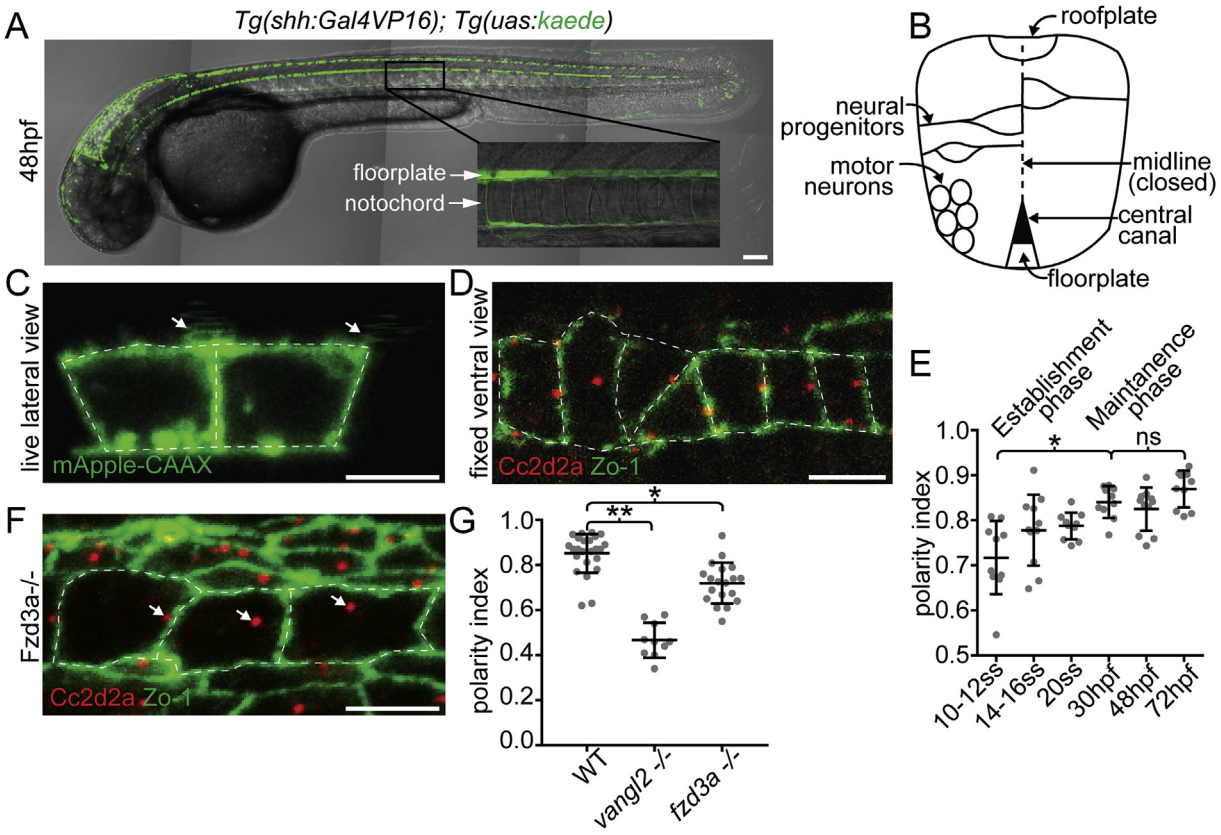

Fig. 1. The floorplate is progressively planar polarized in a Vangl2 and Fzd3a-dependent manner. (A) A 48hpf *Tg:(shh:gal4); Tg(uas:Kaede)* zebrafish embryo expressing Kaede in the floorplate of the neural tube. (B) Schematic of a cross-section of the zebrafish neural tube at 48hpf (not to scale). (C) Single time point from a time lapse of a *Tg(shh:gal4); Tg(uas:mApple-CAAX)* embryo at 48hpf in which two adjacent floorplate cells are expressing membrane-localized mApple-CAAX (green). Posteriorly localized primary cilia (arrows) appear as squiggles due to their rapid motion. (D) Fixed ventral view of a 48hpf WT floorplate co-immunostained with ZO-1 to mark sub-apical tight junctions (green) and Cc2d2a to mark BBs (red). (E) Quantitation of per embryo polarity index from the 10–12ss through 72hpf. Each dot represents the average polarity index of at least 10 cells within a single embryo. Total N = 62 embryos, 1130 cells. *$p < 0.0001$; significance was determined with a Kruskal-Wallis test with Dunn's multiple comparison. (F) Fixed ventral view of a 48hpf *fzd3a*$^{-/-}$ floorplate stained as in D. White dotted line indicates position of cell boundaries, as determined by mApple-CAAX fluorescence (C) or ZO-1 staining (D,F), arrows indicate BB positions. (G) BB polarity indices of WT, *vangl2*$^{-/-}$ and *fzd3a*$^{-/-}$ embryos at 48hpf. Each dot represents the average polarity index of at least 10 cells within a single embryo. Total N = 54 embryos, 448 cells; **$p < 0.0001$; *$p = 0.0018$; significance was determined with a Kruskal-Wallis test with Dunn's multiple comparison. Anterior is to left in all images. Scale bars: 100 μm (A) or 5 μm (C,D,F).

polarized to the anterior and posterior apical sides of floorplate cells, respectively (Davey et al., 2016). We crossed *Tg(shh:gal4)* animals with *Tg(uas:mAppleCAAX)* and *Tg(uas:GFP-Vangl2)* or *Tg(uas:Fzd3a-GFP)* to generate embryos to visualize PCP protein localization (green) relative to the membrane (red) in isolated expressing cells due to mosaic silencing of the UAS-driven transgenes ((Goll et al., 2009); see methods). We found that at 48 hpf GFP-Vangl2 is significantly polarized to the anterior half of the cell ($p = 0.0035$, $n = 54$ cells, 12 embryos) whereas Fzd3a-GFP localizes to the posterior half ($p = 0.0266$, $n = 59$ cells, 25 embryos), when compared to the non-polarized localization of mAppleCAAX ($n = 39$ cells, 20 embryos) (Fig. 2a–c; mAppleCAAX channel not shown). This asymmetry is even more dramatic for GFP-Vangl2 when we considered 1 μm wide areas encompassing the anterior and posterior membranes themselves (mean anterior/posterior (A/P) expression ratio of 1.8 ($p = 0.0154$, $n = 18$ cells, 10 embryos) compared to mAppleCAAX: average ratio of 1.1 ($n = 29$ cells, 13 embryos), Fig. 2d, see methods). Surprisingly, given that Fzd3a is also a transmembrane protein, the Fzd3a-GFP asymmetry we observed in the posterior half of floorplate cells does not appear to be due to enrichment in the posterior membrane, but rather represents an asymmetrically localized *cytosolic* pool of the protein (Fig. 2d).

To examine the localization of this cytosolic pool of Fzd3a-GFP and to correlate it with cellular planar polarity as detected by the position of the primary cilium, we imaged the floorplate in live 48hpf *Tg(shh:gal4); Tg(uas:Fzd3a-GFP); Tg(uas:mAppleCAAX)* embryos (Fig. 2e). Measuring pixel intensity in a 3 μm wide band along the apical surface of the cell (Fig. 2f, see methods), we found that peak apical Fzd3a-GFP localization is highly correlated with the position of the primary cilium at 48hpf ($r^2 = 0.79$, $n = 96$ cells from 16 embryos) (Fig. 2f, Supp Movie 2). Previous studies have identified BB-related roles for core PCP components that localize near the BB (Butler and Wallingford, 2015; Hashimoto et al., 2010; Park et al., 2008; Vladar et al., 2012; Werner and Mitchell, 2012), suggesting that Fzd3a could be influencing primary cilia function within floorplate cells.

Supplementary video related to this article can be found at https://doi.org/10.1016/j.ydbio.2019.04.007.

3.3. Planar polarized Fzd3a and Vangl2 exhibit different dynamics in the floorplate

Live imaging also showed that cytosolic Fzd3a-GFP localizes to highly dynamic puncta (1 punctum defined as a point of local signal intensity ranging from 0.4 to 0.7 μm in diameter that can be traced across multiple timepoints) that congregate around the base of the primary cilium (Supp Movies 2 & 3). We hypothesized that these puncta were Fzd3a-GFP-containing vesicles undergoing MT-based transport during the endocytosis, recycling, and degradation processes of ongoing endocytic flux (Strutt et al., 2011). Therefore, we generated *Tg(shh:gal4);*

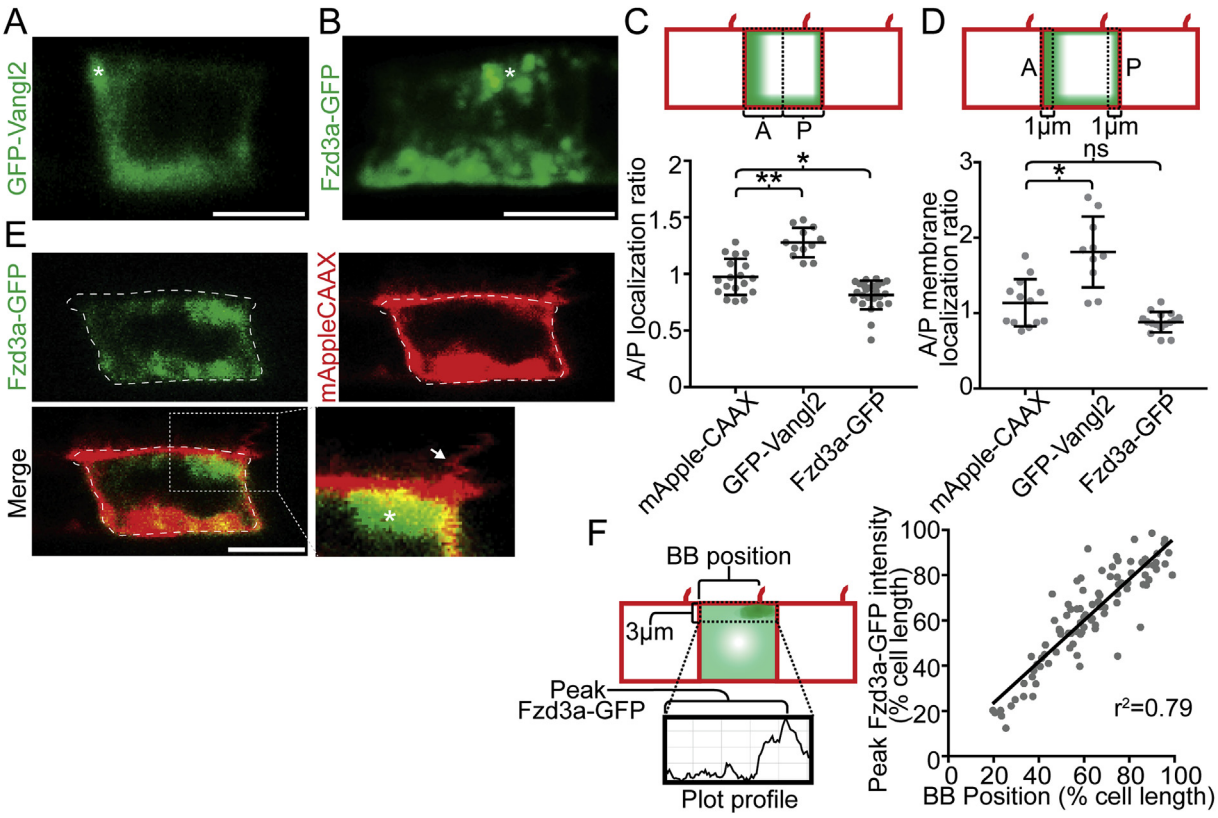

Fig. 2. Vangl2 and Fzd3a localization in the floorplate. (A–B) Live lateral views of 48hpf (A) *Tg(shh:gal4); Tg(uas:GFP-Vangl2)* and (B) *Tg(shh:gal4); Tg(uas:Fzd3a-GFP)* single expressing floorplate cells. Asterisks indicate positions of fusion protein (green) concentration along the apical membrane. (C) Schematic: diagram indicating how total fusion protein localization was measured on anterior vs. posterior cell halves. Graph: quantitation of anterior vs. posterior fusion protein localization in isolated expressing cells. Each dot represents the ratio of the mean fluorescence level within a single cell anterior half divided by the mean fluorescence level of its posterior half. N = 57 embryos, 152 cells; **p = 0.0035; *p = 0.0266; significance was determined with a Kruskal-Wallis test with Dunn's multiple comparison. (D) Schematic: diagram indicating how fusion protein localization was measured on anterior vs. posterior membranes. Graph: quantitation of anterior vs. posterior fusion protein membrane localization in isolated expressing cells. Each dot represents the ratio of the mean fluorescence level along the anterior membrane a single cell divided by the mean fluorescence level along its posterior membrane. N = 39 embryos, 106 cells; *p = 0.0154; significance was determined with a Kruskal-Wallis test with Dunn's multiple comparison. (E) Live lateral views of a 48hpf *Tg(shh:gal4); Tg(uas:Fzd3a-GFP); Tg(uas:mAppleCAAX)* dual transgene expressing floorplate cell. Inset: magnified view of the posterior apical cellular membrane where Fzd3a-GFP (green, asterisk) is concentrated near the base of the primary cilia (red apical extension, arrow). Approximate cell boundaries, as determined by mAppleCAAX expression, indicated by white dotted lines. (F) Schematic: diagram indicating how apically localized cytosolic Fzd3a-GFP levels were quantified (see methods) Graph: correspondence of Fzd3a-GFP peak localization with primary cilium position. Each point corresponds to measurements from a single cell. $r^2 = 0.79$. Anterior to left in all images. Scale bars: 5 µm.

Tg(uas:mApple-Rab5c); Tg(uas:Fzd3a-GFP) and *Tg(shh:gal4); Tg(uas:-mAppleRab7); Tg(uas:Fzd3a-GFP)* embryos and found that Fzd3a-GFP puncta colocalize with both Rab5c- and Rab7-bound vesicles (Supp Movies 4 & 5). As Rab5 is a marker of early endosomes and Rab7 is associated with late endosomes destined for lysosomal degradation, and both have been found to colocalize with PCP proteins in other contexts, these data are consistent with the model that maintenance of core PCP protein asymmetry requires ongoing endocytic flux (Mottola et al., 2010; Strutt and Strutt, 2008) (Strutt et al., 2011).

Supplementary video related to this article can be found at https://doi.org/10.1016/j.ydbio.2019.04.007.

Given the role of the BB as a cellular microtubule organizing center (Badano et al., 2005), and given the role that MTs play in the establishment of PCP via directional trafficking of PCP proteins including Fzd (Harumoto et al., 2010; Matis et al., 2014; Olofsson et al., 2014; Shimada et al., 2006), we examined the organization of MTs in floorplate cells to discover their role in floorplate planar polarization. MTs are composed of αβ-tubulin heterodimers that are modified post-translationally to influence MT stability and function (Westermann and Weber, 2003). The subunits of nascent and dynamic MTs are typically tyrosinated whereas stable MTs become de-tyrosinated and acetylated over time (Bulinski and Gundersen, 1991) (Westermann and Weber, 2003). To identify which MT populations are present within the floorplate at 30 hpf we used established antibody protocols ((McFarland et al., 2017), see methods) to visualize acetylated and tyrosinated tubulin localization. Confocal imaging confirmed the acetylation of primary cilia and revealed a dense cloud of tyrosinated tubulin originating at the base of the primary cilium and extending throughout the cytoplasm of floorplate cells (Supp Fig 1a). These findings are consistent with the BB functioning as the microtubule organizing center (MTOC) at this stage of floorplate development.

Visualizing floorplate MTs by immunohistochemistry does not capture their dynamics or the dynamics of vesicle trafficking along them. Thus, we expressed EB3-mkate2, which marks MT plus-ends (Stepanova et al., 2003) in the floorplate in *Tg(shh:gal4); Tg(uas:EB3-mkate2)* embryos at 30 hpf (Supp Fig 1b, Supp Movie 6) and 48hpf (Supp Movie 7) and observed dynamic EB3 comets spreading throughout the cytoplasm from the posterior apical region of most cells. This region corresponds to the location where the BB is most frequently observed in floorplate cells, again consistent with the BB acting as the primary MTOC at this stage. EB3-mkate2 comets are slowly occluded by the accumulation of EB3-mkate2 along non-centrosomal bundles of MTs at later time points, enabling clear visualization of MT organization *in vivo* (Supp Fig 1b, Supp Movie 8). GFP-Tubulin also localizes to MTs when expressed in floorplate cells but also maintains a diffuse cytosolic population of free GFP-tubulin subunits, making it less ideal for visualizing distinct MT networks (Supp Fig 1b).

Supplementary video related to this article can be found at https://doi.org/10.1016/j.ydbio.2019.04.007.

We next considered whether the dynamic Fzd3a-GFP-containing vesicles we detected in floorplate cells are undergoing MT-based trafficking. By live imaging of Fzd3a-GFP puncta and EB3-mkate2-marked MTs in *Tg(shh:gal4); Tg(uas:EB3-mkate2); Tg(uas:Fzd3a-GFP)* embryos we determined that dynamic Fzd3a-GFP vesicles are indeed strongly associated with MTs by 48 hpf (n = 240 vesicles, 89 cells, 9 embryos). Fzd3a-GFP vesicles move bidirectionally along MT tracks with frequent periods of stalling and switching between MT tracks at junctions (Supp Movie 9; Fig. 3a and b). We sought to characterize the dynamics of the overall vesicular population of Fzd3a-GFP by tracking individual puncta throughout time lapse movies to determine average Fzd3a-GFP vesicle velocities, displacement, and directionality. Overall Fzd3a-GFP vesicle movements measured at 30, 48, and 60 hpf are biased towards the apical membrane of floorplate cells, with 48% of all vesicles tracked (n = 240 vesicles, 89 cells, 9 embryos) moving apically between first and last timepoints measured (Fig. 3c) (see methods). Normalized vesicle displacement was quantified as a measure of perdurance of vesicular motion by dividing the distance between the first and last tracked positions of each vesicle by the total time the vesicle was tracked. Between 30, 48, and 60hpf, average vesicular displacement does not significantly change ($p = 0.1094$, 30hpf compared to 60hpf), with an overall average displacement in a 1-min time interval of 2.4 μm (Fig. 3d). Average vesicle velocity varies across timepoints with vesicles moving significantly faster at 30hpf with an average velocity of 0.09μm/sec (n = 66 vesicles, 27 cells, 4 embryos) compared to 0.07μm/sec at 48hpf ($p = 0.0023$, n = 69 vesicles, 29 cells, 2 embryos) and at 60hpf ($p < 0.0001$, n = 102 vesicles, 33 cells, 3 embryos) (Fig. 3e).

Supplementary video related to this article can be found at https://doi.org/10.1016/j.ydbio.2019.04.007.

Whereas much of Fzd3a-GFP localizes in dynamic MT-associated vesicles, GFP-Vangl2 is predominantly localized to the anterior apical membrane between 30 and 72hpf, and we were unable to detect individual vesicular GFP-Vangl2 undergoing directional movements along EB3-mkate2 labeled MTs (Fig. 2a, d; 3f-g). However, in rare instances we were able to detect individual dynamic vesicular GFP-Vangl2 in Tg(*shh:gal4); Tg(uas-GFP-Vangl2)* embryos, suggesting intracellular trafficking of vesicular Vangl2 is ongoing during PCP maintenance within the floorplate (Fig. 3h; Supp Movie 11). However, the rarity of these vesicles and their susceptibility to photobleaching limited our ability to further investigate the dynamics of vesicular GFP-Vangl2.

Supplementary video related to this article can be found at https://doi.org/10.1016/j.ydbio.2019.04.007.

3.4. Microtubules are required to maintain floorplate PCP

The role of MTs in maintaining PCP protein asymmetric localization after its establishment, or in re-establishing PCP protein asymmetry after it has been disrupted, is controversial (Newman-Smith et al., 2015; Sepich et al., 2011; Shi et al., 2016; Vladar et al., 2012). The defined maintenance phase of floorplate planar polarity from 30 to 72 hpf gave us the opportunity to assess the role of MTs in polarity maintenance in a monociliated cell *in vivo*. We used a modified nocodazole treatment protocol with ice-cold nocodazole (McFarland et al., 2017), which fully disrupts MTs as visualized live in *Tg(shh:gal4); Tg(uas:GFP-Tubulin)* and *Tg(shh:gal4); Tg(uas:EB3-mkate2)* embryos: after 1 h of treatment GFP-Tubulin becomes diffusely cytoplasmic (Supp Fig 2a) and EB3-mkate2 contracts to subapical puncta which correspond to the position of the BB/MTOC (Fig. 4a). In contrast, treating embryos with nocodazole at room temperature for 1 h, even at increased concentrations of 20 ng/ml, only partially disrupts MTs, while treating embryos on ice for 1hr in the absence of the drug has no effect on MTs (Supp Fig 2b). After 1hr cold nocodazole treatment, floorplate cellular planar polarity is lost, with an average BB polarity index of 0.64 ($p = 0.0011$, n = 100 cells, 10 embryos) (Fig. 4b and c). Failure to maintain BB polarization could be because of loss of PCP protein localization and consequent loss of cellular planar polarization, or it may be due to a more direct role for MTs in anchoring the BB to the posterior membrane as has been proposed (Vladar et al., 2012). To investigate the role of MTs in the maintenance of PCP protein asymmetry, we treated *Tg(shh:gal4); Tg(uas:GFP-Vangl2)* and *Tg(shh:gal4); Tg(uas:Fzd3a-GFP)* embryos with cold nocodazole at 30 hpf and examined GFP-Vangl2 and Fzd3a-GFP localization. Surprisingly, after 1hr of treatment, GFP-Vangl2 becomes significantly less polarized to anterior membranes with an A/P membrane ratio of 1.2 ($p = 0.0013$, n = 166 cells, 21 embryos) compared to an A/P membrane ratio of 1.4 in DMSO controls at this stage (n = 202 cells, 24 embryos) (Fig. 4d–f). Thus contrary to previous reports (Shi et al., 2016; Vladar et al., 2012), Vangl2 polarization is actively maintained in a MT-dependent manner. A cytosolic population of GFP-Vangl2 that is faintly detectable around the base of the primary cilium in control embryos becomes progressively concentrated there during nocodazole treatment concurrent with the retraction of MTs to the BB (Fig. 4d,g), consistent with a MT-dependent Vangl2 trafficking mechanism. Together our results suggest that asymmetric distribution of Vangl2 is actively maintained in a MT-dependent manner.

As nocodazole treatment disrupts MTs throughout the entire embryo, the changes we observe in floorplate PCP could be influenced by loss of MTs in other tissues. Therefore, we sought a method to disrupt MT-based vesicular trafficking specifically in the floorplate. p50, or dynamitin, is a subunit of the motor protein Dynein. When overexpressed, p50 functions as a dominant-negative (DN) for dynein-based minus end-directed trafficking of cargo along MTs (Burkhardt et al., 1997; Tsujikawa et al., 2007). We hypothesized that p50 overexpression would consequently affect floorplate PCP. Consistent with this hypothesis, a recent report showed that depletion of the Arl3 GTPase, which is thought to mediate release of cargos from dynein, disrupts the polarized distribution of PCP proteins in the developing mouse epidermis (Bhattarai et al., 2019). p50 expression significantly disrupts BB localization when expressed in the floorplate in *Tg(shh:gal4); Tg(uas:p50p2a-eGFPCAAX)* embryos with an average BB polarity index at 48 hpf of 0.55 ($p < 0.0001$, n = 116 cells, 10 embryos), compared to a BB polarity index of 0.77 in non-expressing cells in the same mosaically-expressing embryo (n = 114 cells, 10 embryos) (Supp Fig. 3a and b). The lower polarity index in non-expressing cells in transgenic p50-expressing embryos compared to non-transgenic embryos may be due to the well-known cell non-autonomous effects of disrupting planar polarity (Adler et al., 2000; Stoller et al., 2018). Importantly, Vangl2 polarization is significantly diminished in the floorplate in *Tg(shh:gal4); Tg(uas:p50p2a-eGFPCAAX); Tg(uas:mkate2-Vangl2)* expressing cells (A-P ratio of 1.4; n = 17 cells, 10 embryos) compared to non-expressing cells (A-P ratio of 1.6; n = 21 cells, 10 embryos; $p = 0.0224$) (Supp Fig. 3c and d). Surprisingly, in *Tg(shh:gal4); Tg(uas:p50p2a-eGFPCAAX); Tg(uas:Fzd3a-mEOS^{red})* embryos, Fzd3a puncta in p50-expressing cells are even more tightly apically associated with the base of the primary cilium than in non-expressing cells, ($r^2 = 0.75$, n = 38 cells, 7 embryos) (Supp Fig. 3e and f), suggesting that other mechanisms than minus-end directed transport may contribute to localization of Fzd3a near the BB. Intriguingly, Arl3 depletion in mouse epidermis resulted in loss of Vangl2 planar polarization but caused an unexpected enrichment of Fzd6 at apical membranes, suggesting conserved underlying trafficking mechanisms (Bhattarai et al., 2019). In sum, disrupting directed trafficking in the floorplate disrupts BB polarity and GFP-Vangl2 asymmetry at the membrane, consistent with a role for MT-dependent transport in the maintenance of PCP in the floorplate. It should be noted that in *Tg(shh:gal4); Tg(uas:p50p2a-eGFPCAAX)* embryos p50 is expressed in floorplate cells before 30hpf, which is the start of what we have defined as the maintenance period of floorplate PCP. Thus, we cannot rule out the possibility that the disruption of vesicular trafficking caused by p50 disrupts the initial establishment of PCP protein asymmetry, rather than its maintenance.

As disruption of MTs or directed trafficking along MTs disrupts GFP-Vangl2 asymmetry and primary cilia positioning, and Fzd3a-GFP traffics

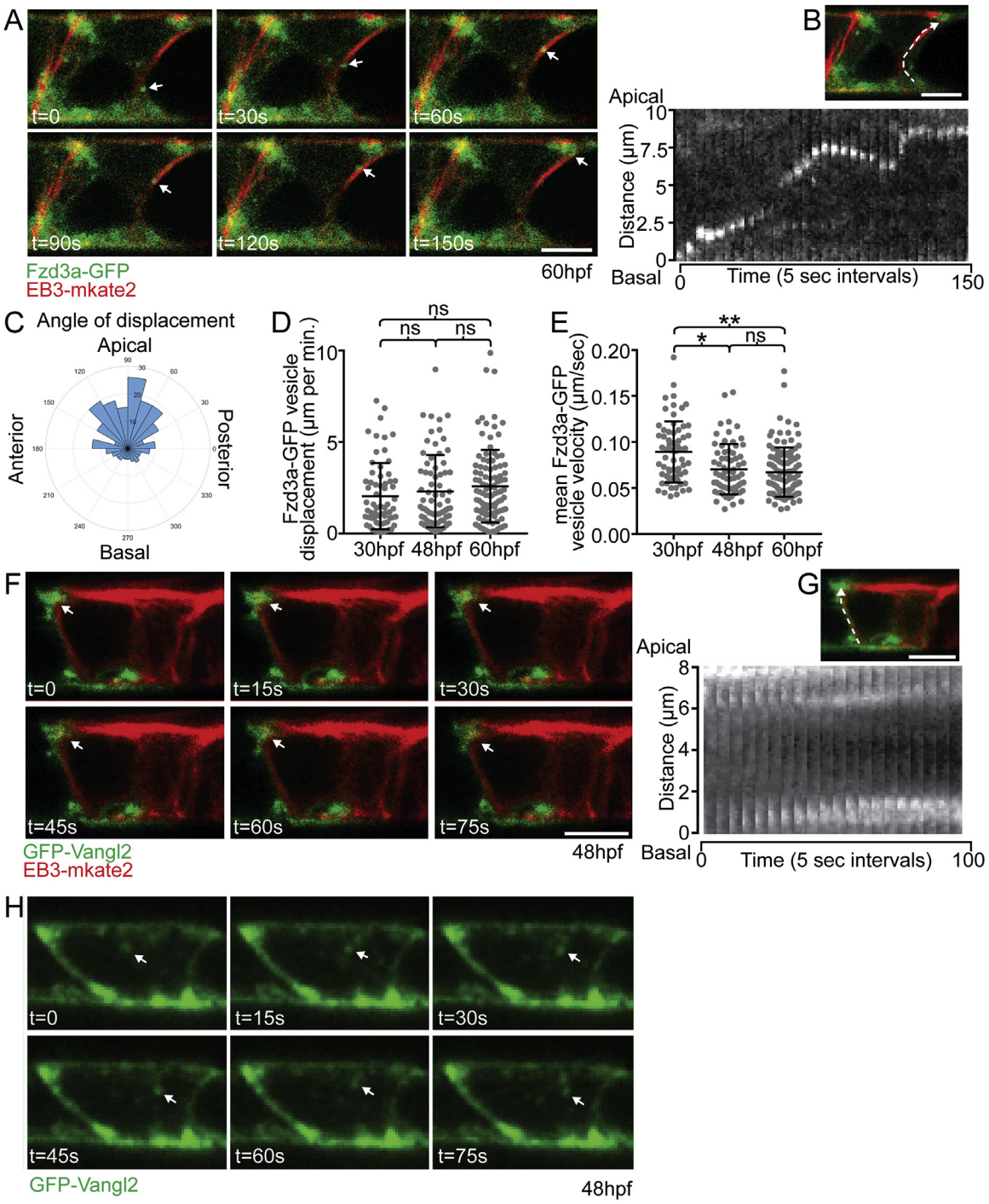

Fig. 3. Fzd3a and Vangl2 trafficking in the floorplate. (A) Single timepoints from a time lapse movie of a 60hpf *Tg(shh:gal4); Tg(uas:Fzd3a-GFP); Tg(uas:EB3-mkate2)* dual transgene expressing floorplate cell in lateral view showing EB3-mKate2-labeled MTs (red) and Fzd3a-GFP vesicles (green). Arrows track an individual Fzd3a-GFP vesicle as it moves in the apical and posterior direction along a MT. (B) inset image: overlay shows measurement path used to generate kymograph. Kymograph: plot showing the apically directed movement of a single Fzd3a-GFP vesicle along a MT polymer. (C–E) Fzd3a-GFP vesicular movements were tracked during 5-s interval time lapse movies of laterally-viewed floorplate cells in *Tg(shh:gal4); Tg(uas:Fzd3a-GFP); Tg(uas:EB3-mkate2)* embryos at 30, 48, and 60hpf. N = 240 vesicles, 89 cells, 9 embryos. (C) Rose plot of final relative displacement angles of individual Fzd3a-GFP containing vesicles between first and last measured positions. (D) Quantitation of individual Fzd3a-GFP vesicle displacement distances between first and last timepoint measured, divided by total tracking time. Significance was determined with a Kruskal-Wallis test with Dunn's multiple comparison. (E) Quantitation of average velocities of individual Fzd3a-GFP vesicles. **$p < 0.0001$; *$p = 0.0023$; significance was determined with a Kruskal-Wallis test with Dunn's multiple comparison. (F) Single timepoints from a time lapse movie of a 48hpf *Tg(shh:gal4); Tg(uas:GFP-Vangl2); Tg(uas:EB3-mkate2)* dual transgene expressing floorplate cell in lateral view. MTs are labeled by EB3-mkate2 (red) and GFP-Vangl2 is shown in green. Arrows indicate GFP-Vangl2 anterior apical localization, which does not change over time. (G) inset image: overlay showing measurement path used to generate kymograph. Kymograph showing the absence of GFP-Vangl2 trafficking along the MT polymer. (H) Single timepoints of a *Tg(shh:gal4); Tg(uas:GFP-Vangl2)* floorplate cell demonstrating a rare example of detectable GFP-Vangl2 cytosolic puncta. Anterior to left in all images. Approximate cell boundaries indicated by white dotted lines. Scale bars: 5 µm.

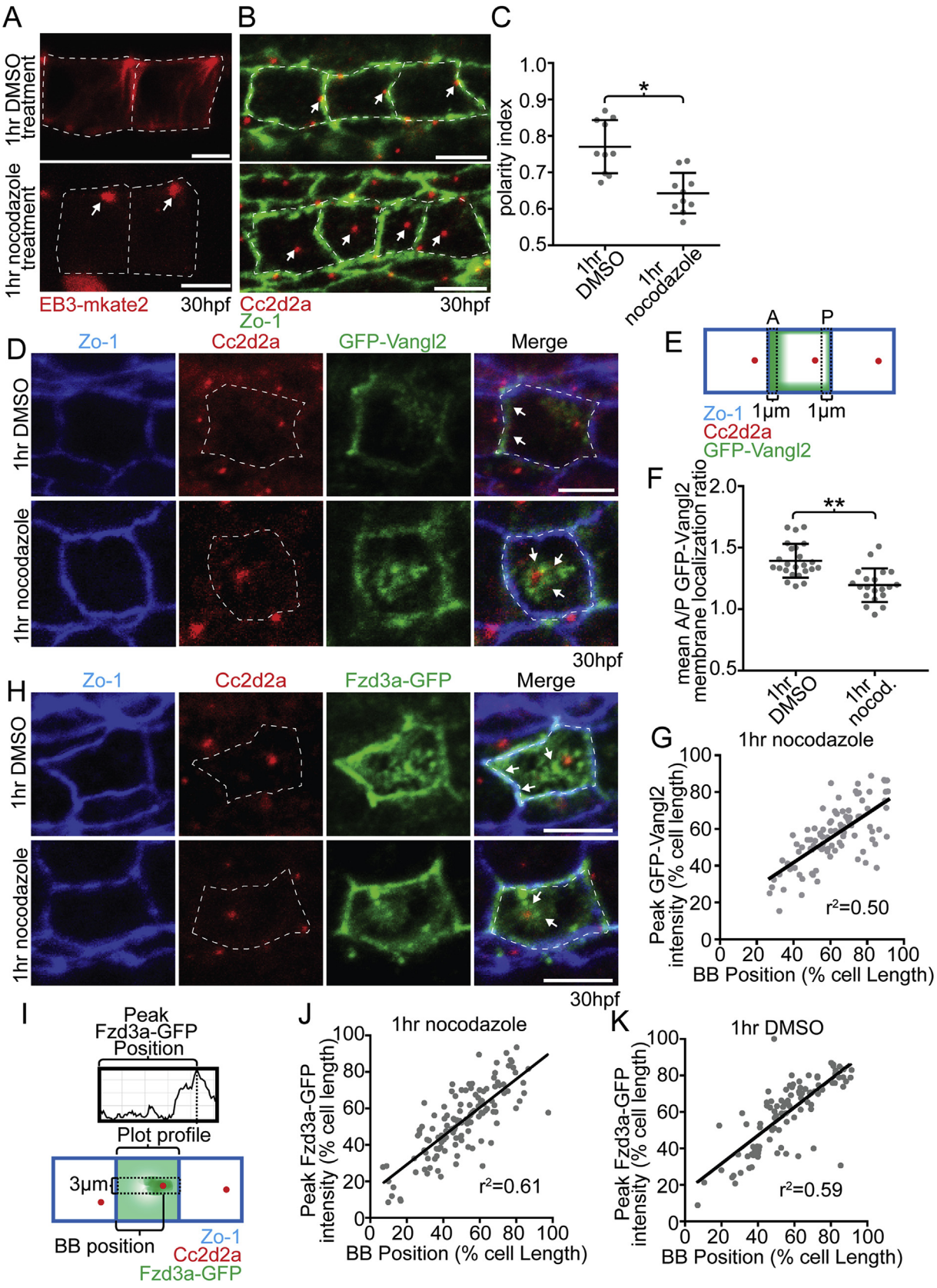

(caption on next page)

Fig. 4. Microtubules are required to maintain floorplate PCP. (A) Live lateral views of floorplate cells expressing *Tg(shh:gal4); Tg(uas:EB3-mkate2)* at 30 hpf. Upon nocodazole treatment EB3-mkate2 labeled MTs collapse to subapical foci near the BB (arrows). (B) Ventral views of Cc2d2a (red) and Zo-1 (green) immunostaining Arrows indicate position of BBs. Nocodazole treatment disrupts the posterior localization of BBs. (C) Quantitation of per embryo average BB polarity index after 1hr DMSO treatment (control) or 1hr nocodazole treatment. N = 200 cells, 20 embryos; *p = 0.0003; significance was determined with Mann-Whitney test. (D) Ventral views of 30hpf *Tg(shh:gal4); Tg(uas:GFP-Vangl2)* embryos. White dotted lines indicate cell boundaries based on ZO-1 staining. Arrows indicate GFP-Vangl2 localization at the anterior membrane in controls and around the BB in nocodazole-treated embryos. (E) Diagram illustrating how anterior and posterior membrane levels of GFP-Vangl2 were measured in fixed ventral floorplate images. (F) Quantitation of per embryo average GFP-Vangl2 anterior vs. posterior membrane localization ratios in isolated floorplate cells expressing *Tg(shh:gal4); Tg(uas:GFP-Vangl2)*. N = 416 cells, 66 embryos; **p < 0.0001, *p = 0.0013; significance was determined with a Kruskal-Wallis test with Dunn's multiple comparison. (G) Graph of the correlation between GFP-Vangl2 and BB localization. After 1hr nocodazole treatment peak GFP-Vangl2 intensity correlates with the position of the BB N = 10 embryos, 100 cells, $r^2 = 0.50$. (H) Ventral views of floorplate cells at 30 hpf immunostained for Fzd3a-GFP (green), Zo-1 (blue) and Cc2d2a (red) after 1hr DMSO treatment (control) or 1hr nocodazole treatment. (I) Diagram illustrating how peak Fzd3a-GFP localization and BB positions were measured. BB distance from anterior membrane was measured compared to overall anterior-posterior cell length. A 3 μm wide ROI centered on the position of the BB was drawn from anterior to posterior membranes. The "plot profile" tool in ImageJ was used to measure average GFP levels across the anterior to posterior cell axis. (J,K) Correlation between Fzd3a-GFP localization and BB position in nocodazole-treated and control floorplate cells. Each data point represents the measurements from a single cell. J: N = 100 cells, 10 embryos; $r^2 = 0.61$; K: N = 100 cells, 10 embryos; $r^2 = 0.59$. Scale bars: 5 μm.

on centrosomal MTs, we next asked how MT loss affects Fzd3a dynamics. In *Tg(shh:gal4); Tg(uas:Fzd3a-GFP)* embryos treated with cold nocodazole, Fzd3a-GFP vesicles remain localized near the base of the now-unpolarized primary cilium, but exhibit reduced motility, consistent with the retraction of MTs toward the BB (Fig. 4h–k; Supp Fig. 4a and b; Supp Movie 12). Whereas Fzd3a-GFP vesicles are highly dynamic in control embryos at 30hpf, in nocodazole-treated embryos they stay relatively stationary over time, with reduced total displacement over time (from 1.8 μm per minute in controls (n = 66 vesicles, 27 cells, 4 embryos) to 0.6 μm per minute in treated embryos (p = 0.0001, n = 79 vesicles, 16 cells, 3 embryos, Supp Fig 4c)) and reduced velocity (from 0.09μm/sec to 0.07μm/sec (p = 0.0043, Supp Fig 4d)). Thus, our results further support the model that Fzd3a actively traffics on MTs during a period of PCP maintenance in the developing floorplate. In summary, BB localization and GFP-Vangl2 asymmetric membrane localization is lost in the absence of MTs, whereas Fzd3a-GFP puncta remain near the (mis-localized) BB even in the absence of MTs or the disruption of minus-end trafficking.

Supplementary video related to this article can be found at https://doi.org/10.1016/j.ydbio.2019.04.007.

3.5. Maintenance of PCP protein polarity does not depend on a polarized BB

It is well established that PCP signaling plays an essential role in the initial polarization of the BB/primary cilium (Song et al., 2010; Borovina et al., 2010; Hashimoto et al., 2010; Vladar et al., 2012; Carvajal-Gonzalez et al., 2016; Davey et al., 2016). However, a reciprocal role for BB polarization in the localization of PCP core components is controversial. A model in which a polarized BB/primary cilium is required for the establishment of PCP protein asymmetry during the formation of the ependymal cells that line the brain ventricles has been proposed (Boutin et al., 2014; Ohata and Álvarez-Buylla, 2016; Ohata et al., 2015); however in other planar polarized epithelia molecular PCP is normal when BB polarization is disrupted (Gegg et al., 2014; Jones et al., 2008; Sipe and Lu, 2011). To examine the relationship between a polarized BB and the maintenance of PCP protein asymmetry in the floorplate, we treated 30hpf embryos with cold nocodazole for 1hr to disrupt MTs, BB polarity and GFP-Vangl2 localization. We then removed the drug and allowed the embryos to recover overnight. After an overnight recovery from nocodazole treatment, EB3-labeled MTs repolymerize throughout floorplate cells (Fig. 5a) and Fzd3a-GFP vesicle dynamics also recover (Supp Movie 13). At 48hpf, when control embryos display a BB polarity index of 0.79 (n = 200 cells, 21 embryos), the BB polarity index in nocodazole-recovered embryos was 0.61 (p < 0.0001, n = 203 cells, 19 embryos), which is not significantly different from the polarity index immediately after nocodazole treatment ended (BB polarity index = 0.60, p < 0.9999, n = 212 cells, 18 embryos, Fig. 5b and c).

Supplementary video related to this article can be found at https://doi.org/10.1016/j.ydbio.2019.04.007.

The failure of BBs to repolarize after the recovery of MTs gave us the opportunity to ask if BB polarization is required for the recovery of asymmetric PCP protein localization, by determining whether GFP-Vangl2 can repolarize to anterior membranes after recovery from nocodazole. Immediately after 1hr nocodazole treatment, floorplate cells exhibited an average GFP-Vangl2 A/P membrane ratio of 1.2 (n = 156 cells, 20 embryos), however GFP-Vangl2 polarization recovered to 1.4 after 3 h of recovery (p = 0.0891, n = 74 cells, 10 embryos), and to 1.5 after overnight recovery (p = 0.0004, n = 169 cells, 20 embryos) (Fig. 5d and e). Furthermore, the dense localization of GFP-Vangl2 near the BB that we detected immediately after nocodazole treatment is no longer present after this recovery period (Fig. 5d). Together these results demonstrate that molecular polarization of the floorplate requires MTs but can be established in the absence of a planar-polarized BB/primary cilium.

4. Discussion

Our work sought to investigate the role of MTs in the maintenance of PCP protein asymmetry and cellular polarity in the floorplate of the developing zebrafish neural tube. We identified two distinct phases of planar polarization: an establishment phase during which the BB becomes progressively localized toward the posterior side of each cell, and a maintenance phase during which BB position is stably maintained. By mosaically expressing fluorescent fusion proteins of the essential PCP components Vangl2 and Fzd3a in the floorplate, we determined that GFP-Vangl2 stably localizes to anterior apical membranes during the maintenance phase and Fzd3a-GFP is predominantly visible in cytoplasmic vesicles that traffic dynamically on MTs and accumulate near the BB. BB posterior localization, GFP-Vangl2 anterior localization and Fzd3a-GFP trafficking are all disrupted when MTs are depolymerized during the maintenance phase. GFP-Vangl2 anterior localization can be re-established during the maintenance phase, indicating an active and ongoing maintenance process dependent on MTs. Finally, re-establishment of polarized GFP-Vangl2 can occur in the context of an unpolarized BB. Below we discuss how our findings differ from existing models and what these differences reveal about mechanisms of planar polarization.

4.1. PCP protein dynamics and localization

Our work has described the dynamics of GFP-Vangl2 and Fzd3a-GFP localization in the planar-polarized floorplate. Our findings are consistent with established PCP models in that subcellular asymmetric localization of core PCP components underlies most planar polarized systems to date. Vangl2 asymmetric membrane localization has been described in many epithelial cell types, and Fzd proteins are known to traffic in vesicles in order to establish planar polarity in fly (Butler and Wallingford, 2015; Shimada et al., 2006). The fact that we were unable to detect Fzd3a-GFP asymmetry at the membrane is not unexpected, as PCP

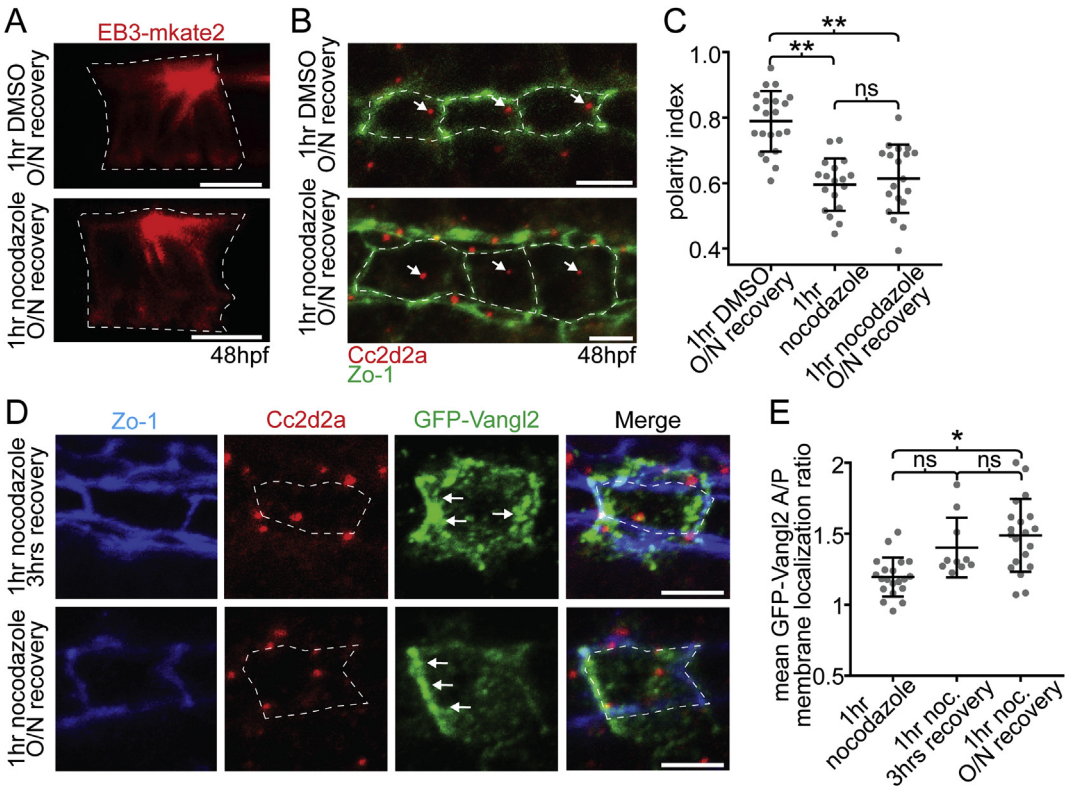

Fig. 5. Maintenance of PCP protein polarity does not depend on a polarized BB. (A) EB3-mkate localization to centrosomal MTs recovers after recovery from nocodazole treatment (compare to Fig. 4A). (B) Ventral images of fixed 48hpf WT floorplates coimmunostained for Cc2d2a (red) and ZO-1 (green). BBs (arrows) remain delocalized after recovery from nocodazole treatment. (C) Quantitation of per embryo average BB polarity index in WT embryos that were treated with either DMSO (control) or cold 5 ng/μl nocodazole for 1hr and then either fixed immediately or allowed to recover overnight. N = 615 cells, 58 embryos; **p < 0.0001; significance was determined with a Kruskal-Wallis test with Dunn's multiple comparison. (D) Ventral images of fixed GFP-Vangl2 expressing floorplate cells in *Tg(shh:gal4); Tg(uas:GFP-Vangl2)* embryos that were treated with nocodazole for 1hr and then recovered for either 3 hrs or overnight. Arrows indicate recovery of asymmetric GFP-Vangl2 localization. Compare to Fig. 4D. (E) Quantitation of GFP-Vangl2 anterior vs. posterior membrane localization ratios after 1hr nocodazole treatment followed by different recovery periods. N = 236 cells, 29 embryos; *p = 0.0004; significance was determined with a Kruskal-Wallis test with Dunn's multiple comparison. White dotted lines mark approximate cell boundaries, based on ZO-1 staining of tight junctions. Scale bars: 5 μm.

protein asymmetries can be quite subtle or undetectable in other contexts (Aw et al., 2016; Strutt and Strutt, 2007; Chien et al., 2015). The colocalization of Fzd3a-GFP with BBs has precedent as multiple PCP proteins have been described near BBs, including Vangl2 in mouse kidney epithelia (Ross et al., 2005) and Dvl2 as well as the PCP effectors like Fuz, In, and Wdpcp in *Xenopus* MCCs (Gray et al., 2009; Kim et al., 2010; Park et al., 2006; Zeng et al., 2010). Fzd3a could be performing multiple roles at the BB as PCP signaling has been implicated in numerous BB-related processes in addition to their translational polarization, including the Dvl-dependent apical docking of BBs (Park et al., 2008) and PCP-dependent coordinated tilting and motility of cilia in multiple systems (Butler and Wallingford, 2015; Hashimoto et al., 2010; Vladar et al., 2012; Werner and Mitchell, 2012).

4.2. Microtubules and maintenance of PCP protein asymmetry

It is well established that MTs are required for the initial establishment of PCP protein asymmetry in both invertebrates and vertebrates (Kim et al., 2018; Matis et al., 2014; Olofsson et al., 2014; Shimada et al., 2006; Vladar et al., 2012). However, few studies have investigated how this asymmetry is maintained once it is established, and what the role of MTs is in PCP maintenance. Where PCP maintenance has been addressed, the weight of evidence suggests that MTs are not required to maintain molecular polarity. Pk2 localization to the aboral side of mature mouse embryo tracheal cells is unaffected by nocodazole treatment (MTECs (Vladar et al., 2012)); similarly, Vangl2 asymmetric localization in the mouse oviduct epithelium is unaffected by nocodazole treatment after polarity is established (Shi et al., 2016). Finally, GFP-Pk anterior localization in the zebrafish neural plate, once established, is unaffected by nocodazole treatment in the zebrafish gastrula (Sepich et al., 2011). In contrast with these studies, we found that both molecular asymmetry, best described by anterior GFP-Vangl2 localization, and cellular asymmetry based on posterior BB localization, are lost rapidly upon MT depolymerization in the floorplate. A number of factors could account for these different outcomes of MT depolymerization, such as difference in cell type and developmental stage. It is also possible, however, that MTs were not fully disrupted in the previous studies. In the MTEC study, nocodazole treatment disrupted dynamic subapical MTs marked by tyrosinated tubulin but did not disrupt more stable ciliary MTs (Vladar et al., 2012). In the mouse oviduct study, nocodazole treatment failed to completely abolish a subapical lattice of MTs that links ciliary BBs, which could be sufficient to enable PCP protein trafficking and maintenance of asymmetry (Shi et al., 2016). Subapical MT networks stabilize over time (Muroyama and Lechler, 2017; Werner et al., 2011) and nocodazole primarily targets more dynamic MTs by binding free tubulin subunits (Baas et al., 2016). Indeed, our own early experiments with nocodazole failed to fully disrupt floorplate MTs or PCP protein localization. It was not until we combined nocodazole treatment with cold temperatures (McFarland et al., 2017), which eliminated both stable MTs and dynamic MT populations within the floorplate, that we observed the effects on molecular polarization that we have described. In sum, our study challenges the model that MTs are dispensable after PCP protein asymmetry has been established by directly visualizing the *in vivo* consequences that MT destabilization has on maintenance of PCP protein distribution and

dynamics.

Given that the BB is a nexus of many MTs within these cells, it is possible that individual PCP protein-containing vesicles transiently accumulate near the BB before they are distributed to individual MTs for directional trafficking towards cell membranes. If this is the case one would predict that the BB has an active role in coordinating the polarized distribution of PCP components throughout the cell. Indeed, when MTs are disrupted we observe that GFP-Vangl2, which normally asymmetrically localizes to anterior membranes, accumulates near the BB. This could indicate that vesicular Vangl2 normally traffics along centrosomal MTs and cannot reach anterior or posterior membranes in their absence. We only rarely detected GFP-Vangl2 puncta within untreated floorplate cells during our analysis, however unlike vesicular Fzd, vesicular Vangl2 is also rarely detected in other models (Shi et al., 2016). We cannot rule out that these differences could be artefactual due to the use of PCP fusion proteins to visualize protein dynamics, but our observations support a model in which both Fzd3a and Vangl2 proteins are actively trafficked along MTs during phases of cellular PCP maintenance.

4.3. The basal body asymmetry and PCP

The links between PCP signaling and BB positioning are complex and not fully understood at a mechanistic level. Though it is well-established that PCP signaling is required for the asymmetric position and orientation of BBs in many epithelia (reviewed in (Carvajal-Gonzalez et al., 2016)), whether the asymmetric position of the BB can reciprocally influence the establishment or maintenance of PCP protein asymmetry is controversial. (This is separate from the question of whether the PCP pathway influences ciliogenesis per se, which is a different debate (Wallingford and Mitchell, 2011)). In the radial glial precursors of ependymal cells that line the brain ventricles, asymmetric BB positioning precedes the asymmetric accumulation of Vangl2, and mislocalization of the BB results in a corresponding mislocalization of Vangl2 (Boutin et al., 2014; Mirzadeh et al., 2010). This has led to a model in which the off-center positioning of the BB/primary cilium (itself the consequence of cerebrospinal fluid flow) could provide the symmetry-breaking event that facilitates the polarized distribution of PCP proteins (Boutin et al., 2014; Ohata and Álvarez-Buylla, 2016; Ohata et al., 2015). This is an attractive model for cells such as the floorplate where the BB serves as the MTOC, and the trafficking of PCP protein-containing vesicles towards an asymmetrically localized MTOC as we have observed could be sufficient to break symmetry. Possibly consistent with this model is the finding that some mutants that disrupt BB positioning in the mammalian cochlea also exhibit disrupted molecular polarization (May-Simera et al., 2015); however most such mutants do not (Gegg et al., 2014; Jones et al., 2008; Sipe and Lu, 2011).

Since nocodazole-induced loss of BB asymmetry in the floorplate corresponded with a decrease of asymmetric GFP-Vangl2 at the membrane, we were curious if BB position could influence PCP protein distribution. Intriguingly, we discovered that restoration of MTs after removal of nocodazole largely restores GFP-Vangl2 asymmetry at the membrane as well as vesicular Fzd3a-GFP dynamics, without rescuing BB asymmetric localization. This decoupling of BB position from GFP-Vangl2 polarization is strong evidence that asymmetric BB position is not required for the re-establishment of PCP protein asymmetry. It is possible that, like in the cochlea, parallel pathways ensure molecular polarization in the absence of a polarized MTOC in the floorplate (Ezan et al., 2013). The MT-dependent processes that re-establish molecular polarization in the floorplate remain to be determined.

Acknowledgements

We would like to acknowledge the many people that have contributed to this work. We thank the members of the Moens lab for many helpful discussions, especially Minna Roh-Johnson who provided comments on the manuscript and Adam Isabella for his aid in generating rose plots. We also thank Lisa Voelker for assistance with analysis of vesicular dynamics, Jarema Malicki for providing the p50 plasmid, and Mary Halloran who offered a critical suggestion regarding MT stability. This work was supported by NIH Grant 5R01NS082567-05.

Appendix A. Supplementary data

Supplementary data to this article can be found online at https://doi.org/10.1016/j.ydbio.2019.04.007.

References

Adler, P.N., Taylor, J., Charlton, J., 2000. The domineering non-autonomy of frizzled and van Gogh clones in the Drosophila wing is a consequence of a disruption in local signaling. Mech. Dev. 96, 197–207.
Aw, Wen Y., Heck, Bryan W., Joyce, B., Devenport, D., 2016. Transient tissue-scale deformation coordinates alignment of planar cell polarity junctions in the mammalian skin. Curr. Biol. 26, 2090–2100.
Baas, P.W., Rao, A.N., Matamoros, A.J., Leo, L., 2016. Stability properties of neuronal microtubules. Cytoskeleton 73, 442–460.
Bachmann-Gagescu, R., Phelps, I.G., Stearns, G., Link, B.A., Brockerhoff, S.E., Moens, C.B., Doherty, D., 2011. The ciliopathy gene cc2d2a controls zebrafish photoreceptor outer segment development through a role in Rab8-dependent vesicle trafficking. Hum. Mol. Genet. 20, 4041–4055.
Badano, J.L., Teslovich, T.M., Katsanis, N., 2005. The centrosome in human genetic disease. Nat. Rev. Genet. 6, 194–205.
Bhattarai, S.R., Begum, S., Popow, R., Ezratty, E.J., 2019. The Ciliary GTPase Arl3 Maintains Tissue Architecture by Directing Planar Spindle Orientation during Epidermal Morphogenesis. Development *in press*.
Borovina, A., Superina, S., Voskas, D., Ciruna, B., 2010. Vangl2 directs the posterior tilting and asymmetric localization of motile primary cilia. Nat. Cell Biol. 12, 407–412.
Boutin, C., Labedan, P., Dimidschstein, J., Richard, F., Cremer, H., André, P., Yang, Y., Montcouquiol, M., Goffinet, A.M., Tissir, F., 2014. A dual role for planar cell polarity genes in ciliated cells. PNAS 111, E3129–E3138.
Bulinski, J.C., Gundersen, G.G., 1991. Stabilization and post-translational modification of microtubules during cellular morphogenesis. Bioessays News Rev. Mol. Cell. Dev. Biol. 13, 285–293.
Burkhardt, J.K., Echeverri, C.J., Nilsson, T., Vallee, R.B., 1997. Overexpression of the dynamitin (p50) subunit of the dynactin complex disrupts dynein-dependent maintenance of membrane organelle distribution. J. Cell Biol. 139, 469–484.
Butler, M.T., Wallingford, J.B., 2015. Control of vertebrate core planar cell polarity protein localization and dynamics by Prickle 2. Development 142, 3429–3439.
Butler, M.T., Wallingford, J.B., 2017. Planar cell polarity in development and disease. Nat. Rev. Mol. Cell Biol. 18, 375–388.
Butler, M.T., Wallingford, J.B., 2018. Spatial and temporal analysis of PCP protein dynamics during neural tube closure. Elife 7, e36456.
Carvajal-Gonzalez, J.M., Mulero-Navarro, S., Mlodzik, M., 2016. Centriole positioning in epithelial cells and its intimate relationship with planar cell polarity. Bioessays News Rev. Mol. Cell. Dev. Biol. 38, 1234–1245.
Chien, Y.-H., Keller, R., Kintner, C., Shook, D.R., 2015. Mechanical strain determines the Axis of planar polarity in ciliated epithelia. Curr. Biol. 25, 2774–2784.
Ciruna, B., Jenny, A., Lee, D., Mlodzik, M., Schier, A.F., 2006. Planar cell polarity signalling couples cell division and morphogenesis during neurulation. Nature 439, 220–224.
Classen, A.K., Anderson, K.I., Marois, E., Eaton, S., 2005. Hexagonal packing of Drosophila wing epithelial cells by the planar cell polarity pathway. Dev. Cell 9, 805–817.
Curtin, J.A., Quint, E., Tsipouri, V., Arkell, R.M., Cattanach, B., Copp, A.J., Henderson, D.J., Spurr, N., Stanier, P., Fisher, E.M., Nolan, P.M., Steel, K.P., Brown, S.D., Gray, I.C., Murdoch, J.N., 2003. Mutation of Celsr1 disrupts planar polarity of inner ear hair cells and causes severe neural tube defects in the mouse. Curr. Biol. CB 13, 1129–1133.
Davey, C.F., Mathewson, A.W., Moens, C.B., 2016. PCP signaling between migrating neurons and their planar-polarized neuroepithelial environment controls filopodial dynamics and directional migration. PLoS Genet. 12, e1005934.
Davey, C.F., Moens, C.B., 2017. Planar cell polarity in moving cells: think globally, act locally. Development 144, 187–200.
Deans, M.R., Antic, D., Suyama, K., Scott, M.P., Axelrod, J.D., Goodrich, L.V., 2007. Asymmetric distribution of prickle-like 2 reveals an early underlying polarization of vestibular sensory epithelia in the inner ear. J. Neurosci. Offic. J. Soc. Neurosci. 27, 3139–3147.
Devenport, D., Fuchs, E., 2008. Planar polarization in embryonic epidermis orchestrates global asymmetric morphogenesis of hair follicles. Nat. Cell Biol. 10, 1257–1268.
Devenport, D., Oristian, D., Heller, E., Fuchs, E., 2011. Mitotic internalization of planar cell polarity proteins preserves tissue polarity. Nat. Cell Biol. 13, 893–902.
Ertzer, R., Muller, F., Hadzhiev, Y., Rathnam, S., Fischer, N., Rastegar, S., Strahle, U., 2007. Cooperation of sonic hedgehog enhancers in midline expression. Dev. Biol. 301, 578–589.
Etheridge, S.L., Ray, S., Li, S., Hamblet, N.S., Lijam, N., Tsang, M., Greer, J., Kardos, N., Wang, J., Sussman, D.J., Chen, P., Wynshaw-Boris, A., 2008. Murine dishevelled 3

functions in redundant pathways with dishevelled 1 and 2 in normal cardiac outflow tract, cochlea, and neural tube development. PLoS Genet. 4, e1000259.
Ezan, J., Lasvaux, L., Gezer, A., Novakovic, A., May-Simera, H., Belotti, E., Lhoumeau, A.-C., Birnbaumer, L., Beer-Hammer, S., Borg, J.-P., Le Bivic, A., Nürnberg, B., Sans, N., Montcouquiol, M., 2013. Primary cilium migration depends on G-protein signalling control of subapical cytoskeleton. Nat. Cell Biol. 15, 1107–1115.
Gegg, M., Böttcher, A., Burtscher, I., Hasenoeder, S., Campenhout, C.V., Aichler, M., Walch, A., Grant, S.G.N., Lickert, H., 2014. Flattop regulates basal body docking and positioning in mono- and multiciliated cells. eLife 3, e03842.
Goll, M.G., Anderson, R., Stainier, D.Y., Spradling, A.C., Halpern, M.E., 2009. Transcriptional silencing and reactivation in transgenic zebrafish. Genetics 182, 747–755.
Goodrich, L.V., Strutt, D., 2011. Principles of planar polarity in animal development. Development 138, 1877–1892.
Gray, R.S., Abitua, P.B., Wlodarczyk, B.J., Szabo-Rogers, H.L., Blanchard, O., Lee, I., Weiss, G.S., Liu, K.J., Marcotte, E.M., Wallingford, J.B., Finnell, R.H., 2009. The planar cell polarity effector Fuz is essential for targeted membrane trafficking, ciliogenesis and mouse embryonic development. Nat. Cell Biol. 11, 1225–1232.
Gubb, D., Garcia-Bellido, A., 1982. A genetic analysis of the determination of cuticular polarity during development in Drosophila melanogaster. J. Embryol. Exp. Morphol. 68, 37–57.
Harumoto, T., Ito, M., Shimada, Y., Kobayashi, T.J., Ueda, H.R., Lu, B., Uemura, T., 2010. Atypical cadherins dachsous and fat control dynamics of noncentrosomal microtubules in planar cell polarity. Dev. Cell 19, 389–401.
Hashimoto, M., Shinohara, K., Wang, J., Ikeuchi, S., Yoshiba, S., Meno, C., Nonaka, S., Takada, S., Hatta, K., Wynshaw-Boris, A., Hamada, H., 2010. Planar polarization of node cells determines the rotational axis of node cilia. Nat. Cell Biol. 12, 170–176.
Heisenberg, C.P., Tada, M., Rauch, G.J., Saude, L., Concha, M.L., Geisler, R., Stemple, D.L., Smith, J.C., Wilson, S.W., 2000. Silberblick/Wnt11 mediates convergent extension movements during zebrafish gastrulation. Nature 405, 76–81.
Jessen, J.R., Topczewski, J., Bingham, S., Sepich, D.S., Marlow, F., Chandrasekhar, A., Solnica-Krezel, L., 2002. Zebrafish trilobite identifies new roles for Strabismus in gastrulation and neuronal movements. Nat. Cell Biol. 4, 610–615.
Jones, C., Roper, V.C., Foucher, I., Qian, D., Banizs, B., Petit, C., Yoder, B.K., Chen, P., 2008. Ciliary proteins link basal body polarization to planar cell polarity regulation. Nat. Genet. 40, 69–77.
Kawakami, K., Shima, A., Kawakami, N., 2000. Identification of a functional transposase of the Tol2 element, an Ac-like element from the Japanese medaka fish, and its transposition in the zebrafish germ lineage. PNAS 97, 11403–11408.
Kim, J.H., Lee, S.-R., Li, L.-H., Park, H.-J., Park, J.-H., Lee, K.Y., Kim, M.-K., Shin, B.A., Choi, S.-Y., 2011. High cleavage efficiency of a 2A peptide derived from porcine teschovirus-1 in human cell lines, zebrafish and mice. PLoS One 6, e18556.
Kim, S.K., Shindo, A., Park, T.J., Oh, E.C., Ghosh, S., Gray, R.S., Lewis, R.A., Johnson, C.A., Attie-Bittach, T., Katsanis, N., Wallingford, J.B., 2010. Planar cell polarity acts through septins to control collective cell movement and ciliogenesis. Science 329, 1337–1340.
Kim, S.K., Zhang, S., Werner, M.E., Brotslaw, E.J., Mitchell, J.W., Altabbaa, M.M., Mitchell, B.J., 2018. CLAMP/Spef1 regulates planar cell polarity signaling and asymmetric microtubule accumulation in the Xenopus ciliated epithelia. J. Cell Biol. 217, 1633–1641.
Kimmel, C.B., Ballard, W.W., Kimmel, S.R., Ullmann, B., Schilling, T.F., 1995. Stages of embryonic development of the zebrafish. Dev. Dynam. Offic. Publ. Am. Assoc. Anat. 203, 253–310.
Matis, M., Russler-Germain, D.A., Hu, Q., Tomlin, C.J., Axelrod, J.D., 2014. Microtubules provide directional information for core PCP function. eLife 3, e02893.
May-Simera, H.L., Petralia, R.S., Montcouquiol, M., Wang, Y.-X., Szarama, K.B., Liu, Y., Lin, W., Deans, M.R., Pazour, G.J., Kelley, M.W., 2015. Ciliary proteins Bbs8 and Ift20 promote planar cell polarity in the cochlea. Development 142, 555–566.
McFarland, R., Brown, S., Vital, E., Werner, J., Brewster, R., 2017. Use of immunolabeling to analyze stable, dynamic, and nascent microtubules in the zebrafish embryo. JoVE 127 e55792-e55792.
Meijering, E., Dzyubachyk, O., Smal, I., 2012. Methods for Cell and Particle Tracking. Elsevier.
Mirzadeh, Z., Han, Y.-G., Soriano-Navarro, M., García-Verdugo, J.M., Alvarez-Buylla, A., 2010. Cilia organize ependymal planar polarity. J. Neurosci. 30, 2600–2610.
Montcouquiol, M., Rachel, R.A., Lanford, P.J., Copeland, N.G., Jenkins, N.A., Kelley, M.W., 2003. Identification of Vangl2 and Scrb1 as planar polarity genes in mammals. Nature 423, 173–177.
Montcouquiol, M., Sans, N., Huss, D., Kach, J., Dickman, J.D., Forge, A., Rachel, R.A., Copeland, N.G., Jenkins, N.A., Bogani, D., Murdoch, J., Warchol, M.E., Wenthold, R.J., Kelley, M.W., 2006. Asymmetric localization of Vangl2 and Fz3 indicate novel mechanisms for planar cell polarity in mammals. J. Neurosci. Offic. J. Soc. Neurosci. 26, 5265–5275.
Mottola, G., Classen, A.K., Gonzalez-Gaitan, M., Eaton, S., Zerial, M., 2010. A novel function for the Rab5 effector Rabenosyn-5 in planar cell polarity. Development 137, 2353–2364.
Muroyama, A., Lechler, T., 2017. Microtubule organization, dynamics and functions in differentiated cells. Development 144, 3012–3021.
Newman-Smith, E., Kourakis, M.J., Reeves, W., Veeman, M., Smith, W.C., 2015. Reciprocal and dynamic polarization of planar cell polarity core components and myosin. eLife 4, e05361.
Ohata, S., Álvarez-Buylla, A., 2016. Planar organization of multiciliated ependymal (E1) cells in the brain ventricular epithelium. Trends Neurosci. 39, 543–551.
Ohata, S., Herranz-Perez, V., Nakatani, J., Boletta, A., Garcia-Verdugo, J.M., Alvarez-Buylla, A., 2015. Mechanosensory genes Pkd1 and Pkd2 contribute to the planar polarization of brain ventricular epithelium. J. Neurosci. Offic. J. Soc. Neurosci. 35, 11153–11168.
Olofsson, J., Sharp, K.A., Matis, M., Cho, B., Axelrod, J.D., 2014. Prickle/spiny-legs isoforms control the polarity of the apical microtubule network in planar cell polarity. Development 141, 2866–2874.
Park, T.J., Haigo, S.L., Wallingford, J.B., 2006. Ciliogenesis defects in embryos lacking inturned or fuzzy function are associated with failure of planar cell polarity and Hedgehog signaling. Nat. Genet. 38, 303–311.
Park, T.J., Mitchell, B.J., Abitua, P.B., Kintner, C., Wallingford, J.B., 2008. Dishevelled controls apical docking and planar polarization of basal bodies in ciliated epithelial cells. Nat. Genet. 40, 871–879.
Ross, A.J., May-Simera, H., Eichers, E.R., Kai, M., Hill, J., Jagger, D.J., Leitch, C.C., Chapple, J.P., Munro, P.M., Fisher, S., Tan, P.L., Phillips, H.M., Leroux, M.R., Henderson, D.J., Murdoch, J.N., Copp, A.J., Eliot, M.-M., Lupski, J.R., Kemp, D.T., Dollfus, H., Tada, M., Katsanis, N., Forge, A., Beales, P.L., 2005. Disruption of Bardet-Biedl syndrome ciliary proteins perturbs planar cell polarity in vertebrates. Nat. Genet. 37, 1135–1140.
Roszko, I., Sawada, A., Solnica-Krezel, L., 2009. Regulation of convergence and extension movements during vertebrate gastrulation by the Wnt/PCP pathway. Semin. Cell Dev. Biol. 20, 986–997.
Sepich, D.S., Usmani, M., Pawlicki, S., Solnica-Krezel, L., 2011. Wnt/PCP signaling controls intracellular position of MTOCs during gastrulation convergence and extension movements. Development 138, 543–552.
Shi, D., Komatsu, K., Hirao, M., Toyooka, Y., Koyama, H., Tissir, F., Goffinet, A.M., Uemura, T., Fujimori, T., 2014. Celsr1 is required for the generation of polarity at multiple levels of the mouse oviduct. Development 141, 4558–4568.
Shi, D., Usami, F., Komatsu, K., Oka, S., Abe, T., Uemura, T., Fujimori, T., 2016. Dynamics of planar cell polarity protein Vangl2 in the mouse oviduct epithelium. Mech. Dev. 141, 78–89.
Shi, X., Garcia 3rd, G., Van De Weghe, J.C., McGorty, R., Pazour, G.J., Doherty, D., Huang, B., Reiter, J.F., 2017. Super-resolution microscopy reveals that disruption of ciliary transition-zone architecture causes Joubert syndrome. Nat. Cell Biol. 19, 1178–1188.
Shimada, Y., Usui, T., Yanagawa, S.-i., Takeichi, M., Uemura, T., 2001. Asymmetric colocalization of Flamingo, a seven-pass transmembrane cadherin, and Dishevelled in planar cell polarization. Curr. Biol. 11, 859–863.
Shimada, Y., Yonemura, S., Ohkura, H., Strutt, D., Uemura, T., 2006. Polarized transport of Frizzled along the planar microtubule arrays in Drosophila wing epithelium. Dev. Cell 10, 209–222.
Sipe, C.W., Lu, X., 2011. Kif3a regulates planar polarization of auditory hair cells through both ciliary and non-ciliary mechanisms. Development 138, 3441–3449.
Song, H., Hu, J., Chen, W., Elliott, G., Andre, P., Gao, B., Yang, Y., 2010. Planar cell polarity breaks bilateral symmetry by controlling ciliary positioning. Nature 466, 378–382.
Stepanova, T., Slemmer, J., Hoogenraad, C.C., Lansbergen, G., Dortland, B., Zeeuw, C.I.D., Grosveld, F., Cappellen, G.v., Akhmanova, A., Galjart, N., 2003. Visualization of microtubule growth in cultured neurons via the use of EB3-GFP (End-Binding protein 3-green fluorescent protein). J. Neurosci. 23, 2655–2664.
Stoller, M.L., Roman Jr., O., Deans, M.R., 2018. Domineering non-autonomy in Vangl1; Vangl2 double mutants demonstrates intercellular PCP signaling in the vertebrate inner ear. Dev. Biol. 437, 17–26.
Strutt, D., Johnson, R., Cooper, K., Bray, S., 2002. Asymmetric localization of frizzled and the determination of notch-dependent cell fate in the Drosophila eye. Curr. Biol. CB 12, 813–824.
Strutt, D., Strutt, H., 2007. Differential activities of the core planar polarity proteins during Drosophila wing patterning. Dev. Biol. 302, 181–194.
Strutt, H., Strutt, D., 2008. Differential stability of flamingo protein complexes underlies the establishment of planar polarity. Curr. Biol. CB 18, 1555–1564.
Strutt, H., Warrington, S.J., Strutt, D., 2011. Dynamics of core planar polarity protein turnover and stable assembly into discrete membrane subdomains. Dev. Cell 20, 511–525.
Tada, M., Smith, J.C., 2000. Xwnt11 is a target of Xenopus Brachyury: regulation of gastrulation movements via Dishevelled, but not through the canonical Wnt pathway. Development 127, 2227–2238.
Tree, D.R., Shulman, J.M., Rousset, R., Scott, M.P., Gubb, D., Axelrod, J.D., 2002. Prickle mediates feedback amplification to generate asymmetric planar cell polarity signaling. Cell 109, 371–381.
Tsujikawa, M., Omori, Y., Biyanwila, J., Malicki, J., 2007. Mechanism of positioning the cell nucleus in vertebrate photoreceptors. Proc. Natl. Acad. Sci. U. S. A 104, 14819–14824.
Vladar, Eszter K., Bayly, Roy D., Sangoram, Ashvin M., Scott, Matthew P., Axelrod, Jeffrey D., 2012. Microtubules enable the planar cell polarity of airway cilia. Curr. Biol. 22, 2203–2212.
Wada, H., Tanaka, H., Nakayama, S., Iwasaki, M., Okamoto, H., 2006. Frizzled3a and Celsr2 function in the neuroepithelium to regulate migration of facial motor neurons in the developing zebrafish hindbrain. Development 133, 4749–4759.
Wallingford, J.B., Harland, R.M., 2001. Xenopus Dishevelled signaling regulates both neural and mesodermal convergent extension: parallel forces elongating the body axis. Development 128, 2581–2592.
Wallingford, J.B., Mitchell, B., 2011. Strange as it may seem: the many links between Wnt signaling, planar cell polarity, and cilia. Genes Dev. 25, 201–213.
Walsh, G.S., Grant, P.K., Morgan, J.A., Moens, C.B., 2011. Planar polarity pathway and Nance-Horan syndrome-like 1b have essential cell-autonomous functions in neuronal migration. Development 138, 3033–3042.

Wang, Y., Guo, N., Nathans, J., 2006. The role of Frizzled3 and Frizzled6 in neural tube closure and in the planar polarity of inner-ear sensory hair cells. J. Neurosci. Offic. J. Soc. Neurosci. 26, 2147–2156.
Werner, M.E., Hwang, P., Huisman, F., Taborek, P., Yu, C.C., Mitchell, B.J., 2011. Actin and microtubules drive differential aspects of planar cell polarity in multiciliated cells. J. Cell Biol. 195, 19–26.
Werner, M.E., Mitchell, B.J., 2012. Planar cell polarity: microtubules make the connection with cilia. Curr. Biol. 22, R1001–R1004.
Westerfield, M., 2000. The Zebrafish Book. A Guide for the Laboratory Use of Zebrafish (Danio rerio), fourth ed. Univ. of Oregon Press, Eugene.
Westermann, S., Weber, K., 2003. Post-translational modifications regulate microtubule function. Nat. Rev. Mol. Cell Biol. 4 (12), 938–948.
Zeng, H., Hoover, A.N., Liu, A., 2010. PCP effector gene inturned is an important regulator of cilia formation and embryonic development in mammals. Dev. Biol. 2 (339), 418–428.